Human–Robot Synchrony: Flexible Assistance Using Adaptive Oscillators

Renaud Ronsse*, Nicola Vitiello, Tommaso Lenzi, *Student Member, IEEE*, Jesse van den Kieboom, Maria Chiara Carrozza, *Member, IEEE*, and Auke Jan Ijspeert, *Member, IEEE*

***Abstract*—We propose a novel method for movement assistance that is based on adaptive oscillators, i.e., mathematical tools that are capable of extracting the high-level features (amplitude, frequency, and offset) of a periodic signal. Such an oscillator acts like a filter on these features, but keeps its output in phase with respect to the input signal. Using a simple inverse model, we predicted the torque produced by human participants during rhythmic flexion–extension of the elbow. Feeding back a fraction of this estimated torque to the participant through an elbow exoskeleton, we were able to prove the assistance efficiency through a marked decrease of the biceps and triceps electromyography. Importantly, since the oscillator adapted to the movement imposed by the user, the method flexibly allowed us to change the movement pattern and was still efficient during the nonstationary epochs. This method holds promise for the development of new robot-assisted rehabilitation protocols because it does not require prespecifying a reference trajectory and does not require complex signal sensing or single-user calibration: the only signal that is measured is the position of the augmented joint. In this paper, we further demonstrate that this assistance was very intuitive for the participants who adapted almost instantaneously.**

***Index Terms*—Adaptation, adaptive frequency oscillator, assist-as-needed, flexibility, human–robot interaction, motor primitive.**

I. Introduction

ONE of the most challenging aims of modern robotics is to improve the quality of humans' daily life [1]. In order to accomplish such an ambitious task, robots should cooperate in synergy with humans while working in direct contact with them. This concept is well exemplified with powered exoskeletons, wearable robots designed to assist humans while performing movements [2], [3].

Exoskeletons can be used to increase the performance of healthy persons (i.e., human augmentation robotics) [4], to retrain the nervous system of people suffering after stroke (i.e., rehabilitation robotics) [5], [6], or to assist people affected by chronic movement disorders or neural lesions (i.e., assistive robotics) [7]. Each of the aforementioned applications requires a specific robotic platform and control scheme. Nonetheless, all wearable devices need to face the crucial issue of the human–robot interface [8].

Ideally, the user should fully control the robot in order to have it synchronized with his/her intentions and, consequently, to benefit from the supplied assistance while performing the movement. A common strategy for the human–robot interface is the so-called "shared control" [9]. This approach allows one to share the cognitive effort needed to control the platform between the user and the controller of the robot. As a consequence, the user is interfaced with the robot through some high-level commands that are interpreted and then executed by the robot.

In the case of wearable robots assisting limb motions, these high-level commands must specify the characteristics (e.g., direction, velocity, and amplitude) of the intended movement. Ideally, the robotic platform should detect the user motion intention and react timely to provide the specific assistance needed by the user in terms of direction and absolute value. At the same time, the learning ability of humans plays a fundamental role in achieving human–robot synchrony. For instance, humans can remodulate their muscle activation patterns in order to cope with and exploit the extra torque provided by the robot [10]. In this way, the user reduces his/her effort without losing control of the movement. For these reasons, the analysis of human–robot interactions requires to investigate the cross adaptation of the two partners: The robot adapts its behavior to the user intentions (i.e., movement characteristics), which in turn adapts his/her behavior to optimize the collaboration with the robot.

A possible way to detect the user intention is through a direct interface with the central or peripheral nervous system [11], [12], as demonstrated on primates to control a multi-DOF robotic manipulator [13]. Furthermore, nerve intraneural electrodes were successfully used to control a hand prosthesis [14]. However, these strategies are highly invasive and implants still lack in duration and reliability [15].

Considering less invasive approaches, a large number of electromyography (EMG) based controllers were proposed in the past years to detect the user motion intention for the control of exoskeletons [16], [17]. These systems correlated the user's

Manuscript received July 15, 2010; revised September 22, 2010; accepted October 17, 2010. Date of publication October 25, 2010; date of current version March 18, 2011. This work was supported by the European Union (EU) through the Evolving Morphologies for Human-Robot Symbiotic Interaction Collaborative Project Specific Targeted Research Projects under Grant FP7-ICT-2007-3-231451. *Asterisk indicates corresponding author*.

*R. Ronsse is with the Biorobotics Laboratory, Institute of Bioengineering, École Polytechnique Fédérale de Lausanne (EPFL), CH-1015 Lausanne, Switzerland (e-mail: renaud.ronsse@epfl.ch).

N. Vitiello, T. Lenzi, and M. C. Carrozza are with the Advanced Robotics Technology and System (ARTS) Laboratory, Scuola Superiore Sant'Anna, I-56025 Pontedera, Pisa, Italy (e-mail: n.vitiello@sssup.it; t.lenzi@sssup.it; carrozza@sssup.it).

J. van den Kieboom and A. J. Ijspeert are with the Biorobotics Laboratory, Institute of Bioengineering, École Polytechnique Fédérale de Lausanne (EPFL), CH-1015 Lausanne, Switzerland (e-mail: jesse.vandenkieboom@epfl.ch; auke.ijspeert@epfl.ch).

Color versions of one or more of the figures in this paper are available online at http://ieeexplore.ieee.org.

Digital Object Identifier 10.1109/TBME.2010.2089629

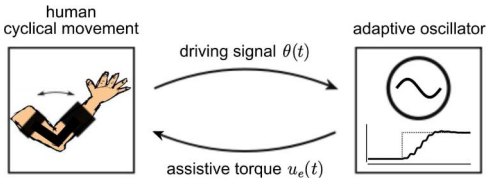

Fig. 1. Sketch of the synchronization between the human joint (elbow in this case) and an adaptive oscillator. The oscillator feeds back some torque $u_e(t)$ to the controlled joint.

EMG with the muscular joint force/torque using either model-based [18] or model-free [19] approaches. These robotic devices provided the wearer with a fraction of the estimated torque to decrease his/her effort. Recently, this approach was used to restore the physiological walking of physically disabled persons [7] and to reduce the metabolic consumption of walking in healthy subjects [20].

Despite these encouraging results, EMG-based approaches have some drawbacks, mainly related to signal acquisition, and user-specific calibration. Electrode positioning, as well as skin condition, greatly affects the recorded signal. As a consequence, EMG-based controllers require not only a long custom calibration for each user but also additional calibrations between and within experimental sessions. Moreover, model-based torque estimation can have poor accuracy and requires large computational effort.

In this paper, we propose an alternative method for providing movement assistance during rhythmic tasks, which predicts the movement trend directly from the joint kinematics. This approach is noninvasive, since it does not rely on any recording of neural commands to the muscles. The only signal that needs to be measured is the assisted joint position. Our method is based on synchronization, a ubiquitous phenomenon in systems biology [21]. Here, synchronization is supposed to happen between two oscillators: a neuromechanical oscillator actually driving the moving joint, and an artificial oscillator providing assistance (see Fig. 1).

The neuromechanical oscillator consists of the limb mechanics and the neural circuits[1] actuating it. The artificial counterpart, providing assistance, is based on an adaptive frequency oscillator,[2] a mathematical tool developed by Righetti *et al.* [27] for various applications [28]: resonance tuning [29], frequency analysis [30], and online learning with robots [31], [32]. An adaptive oscillator is expressed as a dynamical system characterized by a limit cycle whose features (phase, frequency, amplitude, etc.) are changed in adaptation to an external input, i.e., the movement kinematics in this case. Therefore, it reflects the real-time user intention about the performed movement.

The proposed method has been conceived primarily for assistance of the lower leg, given the periodic features of locomotion tasks. Nevertheless, in this study, we will focus on a proof of concept of our approach, i.e., human cyclical movements about the elbow in the upright position. Therefore, the model presented here does not have to deal with complex dynamics due to multijoints coordination or to impacts with the ground, ubiquitous in locomotion. Note, however, that this elbow configuration mimics the inverse-pendulum configuration of legs during the stance phase of walking [33]. This paper mainly establishes that: 1) using an oscillator-based assistance strategy decreases the human effort; 2) the participant always keeps the control of the high-level parameters (namely, movement amplitude and frequency) such that the assistive device flexibly adapts; and 3) our approach requires few user-specific tuning or calibration and is intuitive for the user. Preliminary results were submitted to a conference [34]. This paper provides the first experimental results establishing the adaptive behavior of our algorithm, and further establishes the statistical significance of all results, including more participants.

[1]Possibly based on a spinal central pattern generator (CPG) as discussed for the lower [22] and upper extremities [23]–[26].

[2]For brevity, we will simply refer to this as an *adaptive oscillator* in the rest of this paper. Furthermore, the dynamical system used in this paper has the intrinsic capacity to adapt not only its frequency but also its amplitude and offset, making the term *adaptive oscillator* more generic.

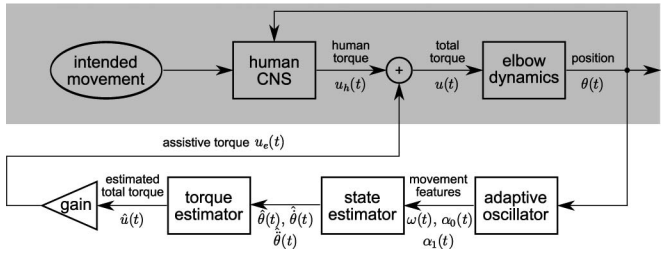

Fig. 2. Block diagram of the integrated system (human + exoskeleton). Each black box is detailed in the text. The shaded area (human + elbow dynamics) does not need to be explicitly modeled.

II. Methods

A. Assistance Using Adaptive Oscillators

Human assistance is provided through an exoskeleton being controlled by an adaptive oscillator [27]. This oscillator is used as state observer (or estimator), in the sense that it acts like a filter to smoothen and anticipate the evolution of the corresponding joint state. Unlike conventional filters, this adaptive oscillator is, however, able to predict an estimate of the state evolution (and the evolution of higher order derivatives) in *real time*, i.e., without delay with respect to the measured output. This is due to the fact that the filter assumes the signal to be periodic, i.e., repetitive. Importantly, this filtering oscillator is currently designed to work only for quasi-sinusoidal signals, and would not work properly with other profiles (see [31] and [32] for adaptation to nonsinusoidal periodic profiles). Finally, the filter continuously adapts to changes in the input signal features, namely, the movement phase, frequency, amplitude, and offset, in the case of a sinusoidal input.

In this study, we focus on the assistance of a simple 1-DOF human joint, namely, the elbow. The fundamental building blocks of the coupled system (human elbow + exoskeleton) are depicted in Fig. 2 and described in the following paragraphs.

1) Human Central Nervous System: The human acts in the loop in order to steer the elbow movement to match with an intended movement (i.e., a sinusoidal movement with a specific

amplitude and frequency in this case). Importantly, an explicit model of this controller, or of the sensory signals being used, is not required for our application. We simply assume that the human provides a torque $u_h(t)$ in order to move the controlled joint.

2) Elbow Dynamics: The elbow dynamics block maps the input torque to an output trajectory, therefore, integrating the different forces acting at the joint level. Again, this block is not explicitly processed in our algorithm, but rather captures the mechanical dynamics of the elbow. An inverse model of this block will be detailed later in this section.

3) Adaptive Oscillator: The adaptive oscillator block is directly adapted from [27]. It is a system of differential equations based on a Hopf oscillator, i.e., a two-state-variables ($x(t)$ and $y(t)$) oscillator having a limit-cycle attractor when $\mu > 0$ and $\gamma > 0$. Moreover, the Hopf oscillator can reach a phase-locked regime with respect to a periodic input $F(t)$ as follows:

$$\begin{aligned}\dot{x}(t) &= \gamma\left(\mu - \left(x(t)^2 + y(t)^2\right)\right)x(t) + \omega(t)y(t) + \nu F(t)\\ \dot{y}(t) &= \gamma\left(\mu - \left(x(t)^2 + y(t)^2\right)\right)y(t) - \omega(t)x(t).\end{aligned} \tag{1}$$

In (1), $\omega(t)$ [rad/s] is the oscillator's intrinsic frequency, and μ and γ determine the oscillator's amplitude and the attractivity of the limit cycle, respectively. In the present experiment, we used $\mu = 1$ (such that the oscillator's intrinsic amplitude equals one) and $\gamma = 8$ (like in [27] and [32]). The learning parameter ν determines the speed of the phase synchronization with respect to $F(t)$. Righetti *et al.* [27] augmented this oscillator to learn the frequency of the input signal $F(t)$, using an integrator whose argument sums up to zero over one period, if $F(t)$ and $y(t)$ have a phase lag of 90° (i.e., if $F(t)$ and $x(t)$ are in phase)

$$\dot{\omega}(t) = \nu F(t)\frac{y(t)}{\sqrt{x(t)^2 + y(t)^2}}. \tag{2}$$

In this paper, we moreover implemented a mechanism to reset the integrator (2), if ever it would be attracted by the movement offset, i.e., the zero frequency. Practically, we reset ω to 2π, if $\omega \leq 0$. Visual inspection of the data revealed that this happened very rarely.

Finally, Righetti and Ijspeert [31] proposed to use this building block to learn the parameters of a sinusoidal input by using the difference between the raw signal $\theta(t)$ (i.e., the elbow position measured by the exoskeleton joint encoder in our case) and the estimated (or learned) signal $\hat{\theta}(t)$ as input, i.e., $F(t) = \theta(t) - \hat{\theta}(t)$. The estimated signal is simply the oscillator output plus an offset term, i.e.,

$$\hat{\theta}(t) = \alpha_0(t) + \alpha_1(t)x(t) \tag{3}$$

where the amplitude α_1 and the offset α_0 can be learned by integrators

$$\begin{aligned}\dot{\alpha_0}(t) &= \eta F(t)\\ \dot{\alpha_1}(t) &= \eta x(t)F(t)\end{aligned} \tag{4}$$

with η being the integrator gain. Due to the intrinsic dynamics, the oscillator time constants are characterized by the gains ν and η. Ideally, these gains should by high enough to smoothly and rapidly drive the oscillator adaptation, but low enough to avoid stability issues. In the present experiment, we used $\nu = 20$ and $\eta = 5$, as found after pilot tests. Fig. 3 shows an example of the oscillator behavior. At time $t = 0$, the input frequency changes. This change is filtered out by the oscillator, which eventually resynchronizes with the new input. The new frequency is learned via the dedicated state variable $\omega(t)$, as shown in Fig. 3(b). Changes in amplitude and offset give rise to similar adaptation of the corresponding state variables. Assuming that the actual input signal is quasi-sinusoidal, the state estimator block easily provides a zero-delay smooth estimate not only of the input signal (3) but also of its velocity and acceleration as follows:

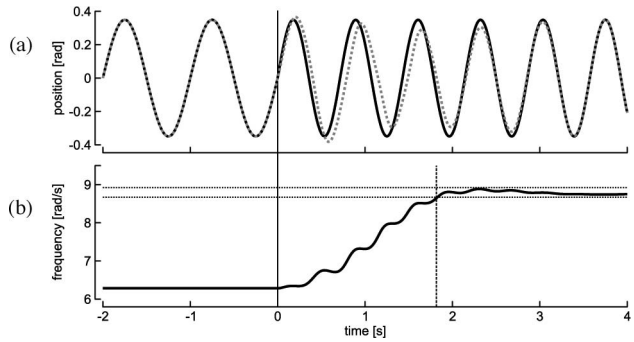

Fig. 3. Example of the oscillator's adaptation dynamics. (a) Oscillator's output $\hat{\theta}(t)$ (dotted gray line) filters out the sudden change in the input $\theta(t)$ (solid black line), i.e., a frequency step at $t = 0$. (b) Corresponding evolution of the learned frequency $\omega(t)$.

$$\begin{aligned}\hat{\dot{\theta}}(t) &= \alpha_1(t)\omega(t)y(t)\\ \hat{\ddot{\theta}}(t) &= -\alpha_1(t)\omega(t)^2x(t).\end{aligned} \tag{5}$$

a) Torque Estimator: We assume that the elbow dynamics can be captured with a simple pendulum model, $I\ddot{\theta}(t) = -mgl\sin\theta(t) - b\dot{\theta}(t) + u(t)$, where I [N·m·s^2/rad], m [kg], and l [m] denote, respectively, the forearm + hand inertia, mass, and equivalent length; b [N·m·s/rad] denotes the elbow viscous damping constant; $g = 9.81$ m/s^2 denotes the constant of gravity; and $\theta(t)$ [rad], $\dot{\theta}(t)$ [rad/s], and $\ddot{\theta}(t)$ [rad/s^2] denote the elbow angular position, velocity, and acceleration, respectively. Finally, $u(t)$ [N·m] denotes the input torque that is applied at the elbow joint, both by the user $u_h(t)$ and by the assistance device $u_e(t)$, i.e., $u(t) = u_h(t) + u_e(t)$. Note that the assistance device mass, damping, and inertia were not considered in this model, assuming the robot is transparent to the user.

The torque estimator block simply retrieves an estimate of the total torque $\hat{u}(t)$ based on an inverse dynamical model of the elbow, i.e.,

$$\hat{u}(t) = mgl\sin\hat{\theta}(t) + b\hat{\dot{\theta}}(t) + I\hat{\ddot{\theta}}(t). \tag{6}$$

Finally, a fraction of this torque is fed back to the user via the assistance device, i.e.,

$$u_e(t) = \kappa\hat{u}(t) \tag{7}$$

where the level of assistance $0 \leq \kappa < 1$. Assuming a stationary sinusoidal movement and a perfect inverse dynamical model (6), such that $\hat{u}(t) = u(t)$, the total torque should emerge from a collaboration between the user (performing $100(1-\kappa)\%$ of the effort) and the assistance device (performing $100\kappa\%$ of the effort). In theory, the stability limit of the assistive controller should be reached at $\kappa = 1$. However, in practice, pilot tests revealed discomfort (like undesired high-frequency oscillations) for κ higher than about 0.6, likely due to neglected dynamics and/or approximations in the inverse model identification (6).

Fig. 4. Front view of a participant wearing the NEUROExos.

B. Participants

Eight healthy right-handed participants took part in the experiment (aged 26–31, weight 51–73, three female, five male). None of them ever experienced the oscillator-based protocol we describe in this paper before the actual acquisition. All participants were volunteers and signed an informed consent form before the experiment.

The parameters of the elbow + forearm inverse dynamical model (6) were individually estimated for each participants, using tables adapted from [35].

1) The forearm mass as 2.2% of the total body weight, i.e., $m = 0.022M$ [kg], where M denotes the total body weight.
2) The forearm equivalent length as 68.2% of the total forearm length, i.e., $l = 0.682L$ [m], where L denotes the total forearm length.
3) The forearm inertia as the product between the forearm mass, and the square of the forearm radius of gyration, i.e., $I = m(0.827L)^2$ [N·m·s^2/rad].

Both M and L were measured for each participant individually. The friction coefficient b was tuned according to the damping factor ζ: $b = 2I\Omega_0\zeta$ [N·m·s/rad], where $\Omega_0 = \sqrt{mgl/I}$ is the resonance frequency of the hanging pendulum (pointing downward). We assumed in our model that $\zeta = 0.8$ for all participants, which is approximately four times higher than documented in the literature (see, e.g., [36]), giving rise to overdamped dynamics. This value was obtained by manual tuning during pilot tests such that it captured residual friction of the forearm part of the exoskeleton, i.e., the part moving with the participant's forearm.

C. Experimental Setup

The assistance device we used in this experiment was the NEUROExos (see Fig. 4), an elbow active orthosis conceived for neurorehabilitation and assistance purposes [37], [38]. The NEUROExos was developed addressing three main design targets. 1) The human elbow anatomy was treated as "loose hinge joint" [39]. Indeed, the rotation axis of the elbow joint changes its orientation along with the elbow flexion–extension motion task. Consequently, NEUROExos was equipped with a 4-DOF passive mechanism to automatically align the rotation axes of the active orthosis and the human elbow. 2) The user–robot mechanical interface was conceived using links with a lightweight double-shell structure, providing a wide comfortable interaction surface. 3) NEUROExos is powered by two antagonist actuators, each composed of a contractile element (hydraulic piston) in series with a nonlinear elastic element. The actuators powered the NEUROExos joint by means of steel wire ropes passing through Bowden cables. The force transmitted by each antagonist tendon cable is sensed by custom force sensors located close to the joint. Since each antagonist unit works as a series-elastic actuator, it was possible to exploit the force sensors to develop two independent closed-loop force controllers [40]–[44]. The force controllers permitted to control the assistance torque $u_e(t)$, with a -3-dB bandwidth of about 15 Hz while providing the NEUROExos with an active back-drivability. The NEUROExos sensors provided measures of the joint (elbow) absolute position and the force transmitted by each tendon cable.

In order to monitor the participant's effort associated with movement performance during all conditions, we recorded the surface EMG activity from the biceps brachii and triceps brachii muscle using bipolar surface Ag/AgCl electrodes (Pirronse&Co., Italy) attached about 2 cm apart along the longitudinal axis of the muscle belly. All the EMG recordings were digitized at 1 kHz using the Telemyo 2400R G2 analog output receiver (Noraxon USA Inc., AZ). Very importantly, note that EMG was not used to control the assistance protocol, but only for *post hoc* assessment of the decrease in effort associated with this protocol.

EMG analog recordings and NEUROExos outputs were synchronized by means of a Labview routine running at 1 kHz on the real-time controller NI PXI-8196 (National Instrument, TX).

D. Experimental Protocol

The participant comfortably sat on a chair, and wore the NEUROExos on their right arm, except during the "*no exo*" condition, which will be detailed in the following paragraph. The NEUROExos was fastened both at the participant upper arm and forearm (see Fig. 4). The NEUROExos support was adjusted to support the participant's arm in the horizontal position, i.e., the shoulder forming an angle of about 90° with respect to the chest in both frontal and transverse planes. Participants were asked to put their forearm in the upright vertical position, and to make cyclical flexion/extension around this position at a target amplitude and pace provided by a computer. Feedback about movement amplitude was provided to the participant via

augmented visual feedback about the movement on a computer screen: a central cursor moved vertically by following the elbow angular displacement, while two peripheral cursors delimited the target movement range. Movement pace was softly constrained by a metronome. Participants were asked to make one full cycle (flexion–extension) between two consecutive beeps. Both the visual feedback and the auditory cuing only provided guidance to the participant to follow the movement features. No corrective actions were applied by the exoskeleton to compensate for errors in movement amplitude or frequency such that the participant always kept the full control of these high-level parameters.

Each participant underwent three types of condition, in the following order.

1) In the "*no exo*" condition, the NEUROExos was actually replaced by a simple 1-DOF goniometer, recording the movement kinematics and providing visual feedback the same way as done by the NEUROExos. The participant had the same posture as described earlier, such that this condition was used as the baseline, to register the kinematics and biceps/triceps EMG corresponding to a control condition. This condition lasted a single trial of about 2 min, at a constant target movement pace of 1 Hz. The last 5 s of acquisition were removed before data processing.
2) In the "constant frequency" condition, participants performed three sequences of five consecutive trials each. Each trial lasted for 60 s and corresponded to a different level of assistance: In trial 1, no assistance was provided [$\kappa = 0$ in (7)]; in trial 2, a "small" amount of assistance was provided ($\kappa = 0.33$, such that the exoskeleton should perform one-third of the total effort); trial 3 was like trial 1 (no assistance), to wash out potential adaptation effects due to the first level of assistance; in trial 4, a "larger" amount of assistance was provided ($\kappa = 0.5$, such that the exoskeleton and the participant should perform half of the total effort each); and trial 5 was again a wash-out trial (see Fig. 8 for the succession of trials). The target movement pace was again constant and equal to 1 Hz. A rest period of a couple of minutes was given between two successive sequences.
3) Finally, participants performed three sequences of the "variable frequency" condition. The succession of assistance levels was similar to the "constant velocity" condition ($\kappa = 0, 0.33, 0, 0.5$, and 0), but this time, the target movement pace varied across the trials. During the first 6 s, the target movement pace was kept constant at 1 Hz (corresponding to about six cycles), then, the target movement pace linearly increased during 12 s to reach 1.4 Hz, then the target movement pace linearly decreased during 24 s to reach 0.6 Hz, then increased again during 12 s to reach 1 Hz, and finally stayed at 1Hz during the last 6 s [see Fig. 10(a)]. These target paces were converted online to varying time intervals that were provided to the participant via the metronome.

The reference amplitude was kept constant across all conditions at $20°$, thus corresponding to a total elbow excursion of about $40°$.

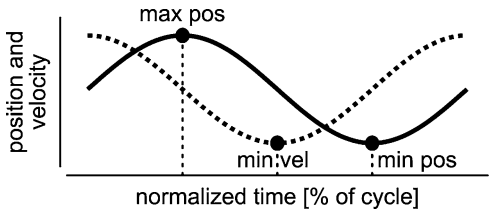

Fig. 5. Kinematics landmarks that were used to analyze the shape of the cycles from the position (solid) and velocity (dotted) profiles: maximum position (max pos), minimum position (min pos), and minimum velocity (min vel). For example, if the cycle was perfectly sinusoidal, max pos $= 25\%$, min vel $= 50\%$, and min pos $= 75\%$.

E. Data Analysis and Statistics

In order to filter the sensor noise for analyzing the movement kinematics, the actual angular position signal $\theta(t)$ that was recorded by the NEUROExos sensor was first offline low-pass filtered[3] (Butterworth, forward and backward in time, third-order, cutoff frequency of 10 Hz), then twice differentiated to get estimates of the angular velocity and acceleration. These two signals were again smoothed using the same Butterworth filter. EMG raw data were processed using the following sequence: 1) high-pass filtering (Butterworth, third order, cutoff frequency of 10 Hz); 2) full-wave rectification using the absolute value of the Hilbert transform; and 3) low-pass filtering (Butterworth, third order, cutoff frequency of 10 Hz). Finally, all biceps and triceps EMG data were independently normalized by the average of the corresponding peak EMG reached during the last 20 cycles of the "*no exo*" condition.

The raw sequence data were separated into trials, of 60 s each (except for the "*no exo*" condition). Then, each trial was separated into cycles using a peak detection algorithm: each cycle was delimited by two consecutive velocity peaks. The ongoing cycle during trial transitions was not included in the analysis. Within each cycle, we computed the following variables.

1) *Average AE* between estimates of the angular position, velocity, and acceleration provided by (3) and (5), and the filtered actual signals. This quantified the performance of the adaptive oscillator to provide smooth but delay-free estimates of these variables.
2) *Cycle amplitude* (half difference between maximum and minimum angular position) and *cycle duration* in order to assess the task fulfillment across the different conditions. We further computed the *location of three movement landmarks* within the cycle, i.e., the maximum position, minimum position, and minimum velocity (see Fig. 5).
3) *Mean and the maximum level of biceps and triceps EMG* in order to assess the influence of the level of assistance on the muscular activity.

Since the number of full cycles within one trial was not always exactly equal to 60, we kept only the data corresponding to the following cycles for displaying the results: the last 20 cycles of the "*no exo*" condition (providing the baseline), the

[3]Importantly, this filtration was ONLY applied for offline statistics and NOT in the online assistance algorithm. The online algorithm received the raw unfiltered position $\theta(t)$ as input to (1), (2), and (4).

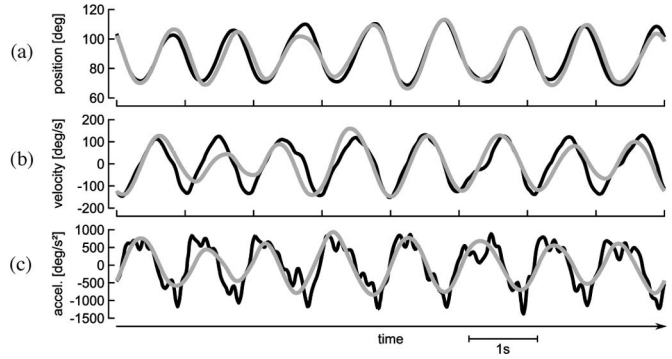

Fig. 6. Comparison between the actual kinematics (black) and the estimated version provided by the AFO (gray) during 8 s of performance in the "*no exo*" condition for a representative participant. (a) Position. (b) Velocity. (c) Acceleration.

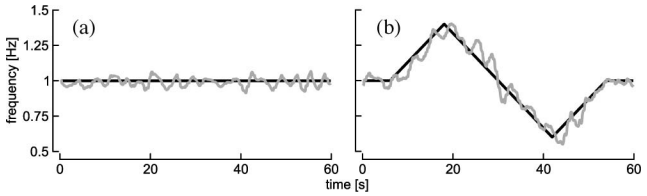

Fig. 7. Evolution of the estimated movement frequency ω throughout a representative trial (gray) of the (a) "constant frequency" condition and (b) "variable frequency" condition. The black line shows the target frequency.

first 20 and last 20 cycles of the "constant frequency" condition, and the middle 48 cycles of the "variable frequency" condition (i.e., corresponding to the nonstationary movement pace). When appropriate, statistics on the steady-state performance was computed on the last 20 cycles of each trial ("*no exo*" and "constant frequency" conditions). Statistical tests revealed that none of the aforementioned variables varied across sequences (two-way ANOVAs using the sequence and the level of assistance as main factors). The effect of the main factor "sequence" and the interaction between both factors never reached significance (all p's > 0.21). Consequently, the sequences were pooled together as within-participant factor, both in the figures and in the statistics. Therefore, statistics are reported as one-way ANOVAs (level of significance set to $p < 0.05$) with the combination of condition and level of assistance as single factor. Four levels were differentiated: 1) "*no exo*" (i.e., $\kappa = 0$); 2) "constant frequency" or "variable frequency" with $\kappa = 0$; 3) "constant frequency" or "variable frequency" with $\kappa = 0.33$; and 4) "constant frequency" or "variable frequency" with $\kappa = 0.5$.

When appropriate, *post hoc* comparisons of the ANOVA levels were tested using the Tukey–Kramer method. All data processing and statistics were computed using MATLAB (the MatWorks, Natick, MA).

III. Results

A. Efficiency of the Adaptive Oscillator

When the movement was (quasi-)stationary, the adaptive oscillator provided delay-free and smooth estimates of the elbow angular position, velocity and acceleration, according to (3) and (5). These estimates are compared to the actual profiles in Fig. 6, over 8 s of performance in the "*no exo*" condition for a representative participant. This figure reveals the high performance of the smoothing based on an adaptive oscillator: The tracking is good, and the estimated signal is not lagging behind the actual one. Also, the oscillator output is a smooth version of the actual kinematics, which is particularly visible for the acceleration.

The oscillator capacity to estimate the movement kinematics was due to the good tracking of the movement features (frequency, amplitude, and offset). Fig. 7 shows the estimated movement frequency ω [from (2)] throughout a representative trial of the "constant frequency" and "variable frequency" conditions. Importantly, the oscillator performance cannot be directly quantified from this figure, since it is impossible to know what was the exact instantaneous frequency of the participant forearm during the movement execution.

The absolute error (AE) between actual and estimated kinematic variables were computed and averaged within each cycle. This is shown in Fig. 8 for both the "*no exo*" condition and the "constant frequency" condition. In the "*no exo*" condition, the mean AE in position [see Fig. 8(a)] was about 1.8°, i.e., 8.9% of the movement amplitude; the mean AE in velocity [see Fig. 8(b)] was about 23.3°/s, i.e., about 18.6% of the velocity amplitude; and the mean AE in acceleration [see Fig. 8(c)] was about $192.8^\circ/\text{s}^2$, i.e., about 32% of the acceleration amplitude. In the "constant frequency" condition, each change in assistance factor was followed by a deterioration of the tracking quality. Focusing on steady-state performance (last cycles), an ANOVA showed significance for all three variables (position: $F(3, 28) = 30.9$; velocity: $F(3, 28) = 30.6$; acceleration: $F(3, 28) = 6.5$; all p's < 0.002), revealing that the estimates in steady-state behavior were more reliable in the "constant frequency" condition than in the "*no exo*" condition, and were more reliable with higher levels of assistance within the "constant frequency" trials.

Worse estimates were obtained during the transient epochs because the movement was slightly changed: in the first cycles with assistance, participants accelerated the movement, before managing to retrieve the metronome pacing, while in contrast, the first cycle of the "wash-out" trials corresponded to slower movements [see Fig. 8(d)]. Steady-state performance of the estimator was reached again after 5–10 cycles.

B. Accuracy and Kinematic Profile Across Conditions

In order to establish that the participants correctly fulfilled the task, and were not perturbed by the exoskeleton mechanics and/or the assistance provided during the corresponding trials, we computed the movement amplitude and duration of each cycle. These variables are shown in Fig. 8(d) and (e) for the "*no exo*" condition and the "constant frequency" condition. As already mentioned earlier, the figure reveals a transient effect due to the adaptation to the assistance torque: the movement amplitude increased for one cycle, then decreased, and was stabilized within about 5–10 cycles, while the cycle duration rapidly decreased (corresponding to faster movements) and reached again

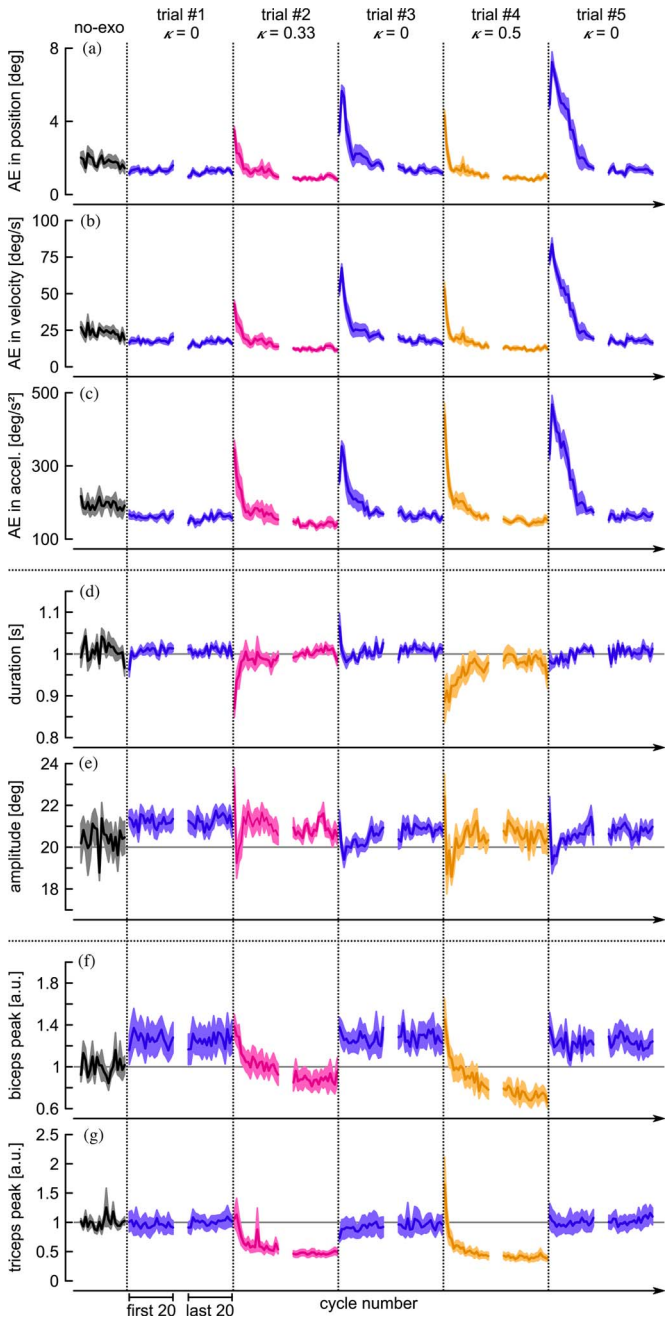

Fig. 8. Cycle-by-cycle evolution of different variables. AE of the oscillator-based estimates of the (a) position, (b) velocity, and (c) acceleration. Movement performance in term of (d) cycle duration and (e) amplitude. Maximum of the measured EMG for the (f) biceps and (g) triceps. The panels show the last 20 cycles of the "*no exo*" condition (black), and the first and last 20 cycles of each trial of the "constant frequency" condition (trials 1, 3, and 5 in blue, trial 2 in purple, and trial 4 in orange). The three sequences were pooled together in the "constant frequency" condition. Shaded areas represent the between-participants SEM.

the target pace after about 5–10 cycles. Some transients are also visible at the beginning of the "wash-out" trials (3 and 5), but they disappeared more rapidly. We designed one-way ANOVAs on the steady-state performance with the condition/level of assistance as the unique factor. None of them reached significance (all p's > 0.1), revealing that the steady-state cycles had the same amplitude and duration in the three levels of assistance of the "constant frequency" condition as within the "*no exo*" condition.

Looking more into the details of possible kinematic changes across conditions, we computed the location (in cycle %) of specific movement landmarks within each cycle (see Fig. 5). Only one of these landmarks significantly changed across the same four conditions, albeit just below the statistical threshold: the minimum velocity was reached earlier in the cycle in the "*no exo*" condition than in the "constant frequency" condition ($F(3, 28) = 3.3, p < 0.04$), at least with $\kappa = 0$ (*post hoc*). This difference reflects that the velocity profile was actually more symmetrical in the "constant frequency" condition than in the "*no exo*" condition.

C. Assistance as a Marked Decrease in EMG

The most striking difference between the performance in the different conditions and levels of assistance was visible in the EMG profiles developed by the participants. Fig. 8 shows the evolution of the EMG peak for the biceps [see Fig. 8(f)] and triceps [see Fig. 8(g)] across the cycles in different conditions. It was normalized for each participant to oscillate around 1 in the "*no exo*" condition. Two important results are visible in this figure: 1) wearing the exoskeleton without assistance (difference between the "*no exo*" condition and the "constant frequency" condition with $\kappa = 0$) induced larger biceps activity, this being certainly due to the exoskeleton forearm's mass and inertia, which were not compensated in that mode and that mainly loaded the joint flexor and 2) providing assistance (both $\kappa = 0.33$ and $\kappa = 0.5$) progressively induced a marked decrease in peak EMG. The highest level of assistance we tested ($\kappa = 0.5$) corresponded to a decrease of about 26% in the biceps peak EMG, and 59% in the triceps peak EMG with respect to the "*no exo*" condition. Fig. 8(f) and (g) also reveals that reaching the reduced level of EMG when assistance was provided took between 10 and 20 cycles for the participants.

Focusing on the steady-state performance, statistics were designed in order to establish the significance of the EMG peak decrease. One-way ANOVAs with the condition/level of assistance as single factor were designed. Both ANOVAs were clearly significant: biceps, $F(3, 28) = 8.5$; triceps, $F(3, 28) = 19.5$; both p's < 0.0003. *Post hoc* tests in the biceps peak EMG revealed a significant decrease between the no assistance ($\kappa = 0$) "constant frequency" trials, and the augmented (both $\kappa = 0.33$ and $\kappa = 0.5$) "constant frequency" trials. The decrease was not significant with the "*no exo*" condition due to the load caused by the exoskeleton forearm. The effect was even clearer in the triceps: *post hoc* comparisons reached significance between any of the nonaugmented trials ("*no exo,*" and "constant frequency," $\kappa = 0$) and any of the augmented one ("constant frequency," $\kappa = 0.33$ and $\kappa = 0.5$). Despite a trend visible in Fig. 8, the difference between the two augmented conditions did not reach significance for neither the biceps nor the triceps.

Fig. 9 shows the steady-state EMG profiles normalized over the whole cycle, by resampling over 101 equally spaced points. The decrease in peak EMG, as reported earlier, is again visible.

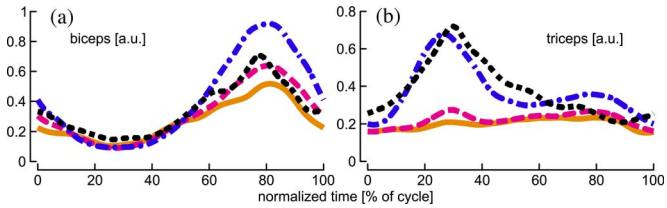

Fig. 9. Steady-state EMG profiles [(a) biceps and (b) triceps] of the "*no exo*" condition (dotted black), and the "constant frequency" condition ($\kappa = 0$, dashed-dotted blue; $\kappa = 0.33$, dashed purple; $\kappa = 0.5$, solid orange). These profiles were obtained by resampling the actual trajectories over 101 equally spaced points for each cycle, then averaging for each of the 101 points.

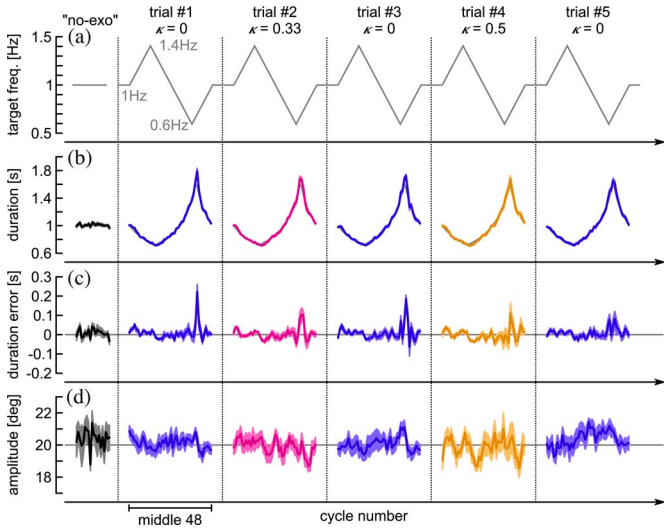

Fig. 10. (a) Target frequency and (b) movement performance in term of cycle duration (c) duration signed error and (d) amplitude. The figure shows the last 20 cycles of the "*no exo*" condition (black), and middle 48 cycles of each trial of the "variable frequency" condition (trials 1, 3, and 5 in blue, trial 2 in purple, and trial 4 in orange). (b) also shows the target cycle duration in gray, thus corresponding to the inverse of the target frequency. The three sequences were pooled together in the "variable frequency" condition. Shaded areas represent the between-participants SEM.

Fig. 9 also shows that the whole EMG profiles actually flatten out when assistance was provided. Consequently, testing the mean level of EMG across conditions gives rise to very similar results as those reported for the peak.

D. Flexibility With Modulations in Movement Frequency

Participants performed three sequences of a nonstationary condition at the end of the session. In this condition, the target pace was not constant anymore, but varied along a triangular wave (except during short epochs at the beginning and end of each trial) [see Fig. 10(a)] in order to establish that the participant kept the possibility to modulate the movement although receiving assistance. Whether our assistance method was still effective during these nonstationary trials is also investigated in this section.

Fig. 10 shows—like Fig. 8(a)–(c) in the "constant frequency" condition—the evolution of the cycle duration and amplitude across the cycles in the "variable frequency" condition. Fig. 10(b) also shows the target duration, thus corresponding

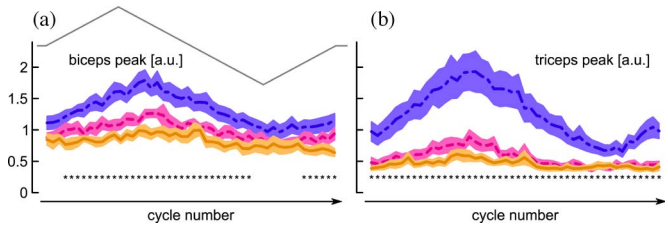

Fig. 11. Maximum of the measured EMG for the (a) biceps and (b) triceps. The figure shows the middle 48 cycles of each trial of the "variable frequency" condition (trials 1, 3, and 5, $\kappa = 0$, pooled in dashed-dotted blue, trial 2, $\kappa = 0.33$, in dashed purple, and trial 4, $\kappa = 0.5$, in solid orange). The three sequences were pooled together. Shaded areas represent the between-participants SEM. The stars denote the cycle for which the one-way ANOVA (level of assistance as factor) was significant with $p < 0.05$. The gray inset shows the variation of the target frequency [see Fig. 10(a)].

to the inverse of the target frequency represented in Fig. 10(a). This illustrates that participants performed well in this condition, moving with a constant amplitude, but varying the cycle duration. Finally, Fig. 10(c) shows the error between the target and the actual duration, reflecting that the cycle duration slightly diverged from the target for slow durations. The variability of this error depended on the condition/level of assistance (same four levels as earlier), as assessed by a one-way ANOVA, although it was near the statistical threshold: $F(3, 28) = 3.7$, $p < 0.03$. *Post hoc* analysis only revealed a significant difference between the "*no exo*" condition and the "variable frequency" condition with $\kappa = 0.5$, this last being more variable. In sum, participants performed the tracking of the target pace with the same level of accuracy in the "variable frequency" condition, whatever be the level of assistance. This performance was also very similar to the tracking performance in the standard condition, i.e., not wearing the exoskeleton.

The adaptive oscillator managed to track the movement parameters with the same level of performance as within the "constant frequency" condition, although with some delay caused by the adaptation dynamics (see Fig. 7(b) for a representative trial showing the frequency estimate). The resulting estimates of the movement kinematic profiles were consequently very good as well. These data are not shown for the sake of brevity, but this will be indirectly proved by showing again a marked decrease in the EMG profiles with assistance, therefore, illustrating the proper working of the oscillator-based torque estimator.

Fig. 11 shows the evolution of the EMG peak across the cycles for the three levels of assistance. The graphs were superimposed to facilitate the visual comparison between the different levels of assistance. It clearly appears that the assistance torque facilitated the movement, since both the biceps and the triceps EMG decreased when some assistance was provided. The EMG peaks also varied depending on the target pace, since faster movements required bigger effort. Due to this modulation, it did not make sense to average the data to compute ANOVAs. Therefore, we computed a one-way ANOVA for each cycle, with the level of assistance as single factor (three levels). Stars in Fig. 11 indicate the cycles for which the ANOVA was significant with $p < 0.05$, i.e., all for the triceps, and all but the slowest cycles for the biceps. In sum, this illustrates that the exoskeleton still provided

assistance to the participant when the movement pace was not stationary.

IV. Discussion

This paper introduces a new method for providing assistance during the execution of rhythmic movements, based on the synchronization between the user's movement and an adaptive oscillator. Synchronization between the user and a compliant robot is an important issue when both have to act in synergy. Aoyagi *et al.* [45] showed that a synchronization mechanism was necessary to control a lower leg highly compliant exoskeleton, even if it played back the average trajectory recorded on the participant itself during free walking. The frequency adaptation mechanism they used was based on a heuristic approach, while here we propose to consider the biological joint controller (i.e., the CPG) and its assistive artificial counterpart as two oscillators whose synchronization is achieved through dynamical coupling. In our approach, the adaptive oscillator is used as a state observer (or estimator), in the sense that it acts like a filter on the input signal. Interestingly, Kuo proposed a similar role for the biological oscillator (i.e., CPG) during execution of rhythmic movements [46].

The proposed method, primarily thought for locomotion tasks, is validated here by taking into account a cyclical movement of the human elbow around the upright position. The input signal (i.e., elbow position) is assumed to contain a single harmonic such that a single specific oscillator is used accordingly. Experimental results show that the pattern executed by the participants is not perfectly sinusoidal, although Fig. 6 reveals that the adaptive oscillator output captures only the main harmonic of the input signal (this is particularly visible from the acceleration profile). Moreover, the inverse model that is used to compute the torque needed to move the exoskeleton and the user's forearm is only a rough estimate of the actual dynamics. In fact, static friction and stiffness were neglected, and the user's anthropometric parameters (i.e., upper limb mass, inertia, and length) were crudely estimated based on Winter's standard tables [35]. Despite these shortcomings, the method is efficient, since all participants were able to flexibly adapt and take advantage of the assistance they received. This robustness is due to the fact that the assistive algorithm is designed to amplify the user torque. Even if the inverse model is not accurate, the user will nevertheless receive some assistance (with level $\neq \kappa$). The participant comfort is optimal, if both torques are in phase.

Besides the capability of the control system to learn the user's movement features and to adapt to their changes, the learning ability of humans also plays a fundamental role. Not only does the assistive exoskeleton adapt its behavior to the user's intention but also the user itself adapts its behavior to the provided assistance, as shown by the remodulation of the EMG activity. Regarding the kinematic profiles, Fig. 8(a)–(c) shows that switching the assistance ON and OFF induces some transients in the quality of the position–velocity–acceleration estimates. This is likely due to the fact that the movement itself changes during these transitory phases. For example, switching the assistance ON makes all participants willing to accelerate the movement, and it takes a few cycles to retrieve the nominal tempo. Due to the oscillator inertia, which depends on the adaptation parameters, these abrupt changes require about ten cycles for the oscillator to get back to the steady-state level of performance. Analysis of the pattern kinematics further reveals that the movement is more symmetrical (and thus more sinusoidal) when assistance is provided. We believe this is an effect of the assistance itself, which is designed assuming sinusoidal movement, and in turn, provides a quasi-sinusoidal torque. Nonetheless, the executed pattern stays very similar across conditions.

Further insights about the cross-adaptation raise from the analysis of the muscles activation. The most striking difference between the not assisted and assisted conditions is the surface EMG measured for the biceps and triceps. Not only do we demonstrate a reduction of the EMG level when the assistance is provided, but we also show that this level goes below the level of the control condition, where the participants do not wear the exoskeleton. Few robotic systems in the state of the art reached similar performances [2], [20], [47], [48]. Our method is the first one that obtains similar results without being controlled by surface EMG, and therefore, avoiding the associated complex calibration and sensing issues.

Adaptation to novel dynamical environments has been extensively described in the motor control literature (see, e.g., [49]–[51]). In this study, we also demonstrate adaptation mechanisms to a novel dynamical environment, although the force field acting on the participant joint is created by the joint movement itself. Moreover, the adaptation time constants measured here are surprisingly small (about ten cycles), and are actually in the same order of magnitude as the adaptation time constant of the oscillator itself.

The results of the nonstationary trials demonstrate that the participants keep the full control of the high-level features of the movement. In particular, we show that they are able to modulate the movement frequency along the trial, while still receiving a substantial amount of assistance. To the best of our knowledge, this is the first time this result has been achieved without needing to sense the surface EMG of the muscles actuating the corresponding joint. The proved adaptivity of the proposed approach in the nonstationary condition is encouraging for the development of novel rehabilitation protocols in which the reference trajectory is not prespecified, but adapts to the user.

Complementing other approaches based on compliance [5], [6], [52], [53], adaptation [5], [54], or adaptive learning of a dynamical model for the task at hand [55], our method opens new perspectives for providing assistance-as-needed based on movement primitives. The concept of movement primitive has been broadly emphasized to account for the organization of complex movements in biology [56], modeling [57], and robotics [58]. In this paper, we propose a very simple rhythmic primitive, i.e., the adaptive oscillator, such that we obtain encouraging results for a particular rhythmic movement, both in steady state and for gently varying conditions. The transfer of our approach for designing novel rehabilitation protocols could, for example, be beneficial for patient suffering from muscular weakness. Indeed, our algorithm both smoothens out the movement kinematics and provides assistance on demand without the need of a reference

trajectory. Concretely, it could be possible to design a rehabilitative protocol to provide assistance-as-needed by regulating the gain κ (the fraction of torque fed back to the patient) on the basis of the ongoing performance. For example, in the first phase of the therapy, when the patient has a lower motion capability, the rehabilitative device provides a high assistance in order to improve the movement performance (e.g., range of motion). Then, at a later stage, it gradually reduces the assistance in order to promote the effort of the patient and, consequently, improve the efficiency of the rehabilitative therapy. Eventually, negative gains could also be used to make the task more difficult. Furthermore, the degree of assistance could also be modulated *within* the cycles, e.g., to provide different support for different phases of the gait, using a phase estimate directly from the adaptive oscillator (1).

Few rhythmic movements are performed by the upper limbs in daily life situations: examples mainly relate to sports, like rowing, or entertainment, like drumming or juggling [59]. Nevertheless, this paper focuses on assistance of the forearm, providing a proof of concept while avoiding complex issues due to coordination or complex dynamics. Future work will focus on adaptation of this method to more functional tasks, like, e.g., walking. This would require careful explorations dealing with nonsinusoidal patterns, interactions with the ground, and coordination between multiple joints. The first issue could be solved by augmenting the filter with a pool of adaptive oscillators, each learning a different harmonic [31], or using a nonlinear kernel filter to shape the signal envelope [32]. Issues related to ground contacts could be solved by developing a model-free version of our approach. Finally, a more sophisticated solution will have to be found to avoid the tracking of the offset (low frequency) component by the oscillator, since resetting the oscillator frequency might create discomfort in a walking experiment.

V. Conclusion

In this paper, we proposed a new method for providing assistance during the execution of rhythmic movements, focusing on the elbow as a proof of concept. Our approach was based on an adaptive oscillator [27], which acted as a state observer (or estimator) to learn and smoothen the high-level features of the signal of interest, but keeping the output in phase with the input. As main results, we showed that 1) the muscles EMG decreased when the assistance was switched ON, revealing that the participants produced less effort to perform the same movement; 2) participants nevertheless kept full control of the movement features, since they were able to modulate the movement frequency online; 3) even in this nonstationary condition, participants still received assistance; and 4) the human adaptation to this assisted environment was surprisingly fast, about ten cycles, and required simple sensors (only the raw assisted joint position needs to be measured) and only crude modeling of the joint dynamics. These results illustrated the cross adaptation between the participant and the assistance protocol: not only the oscillator adapted to the participant behavior but also that the participant adapted to the assisted regime, by reducing both biceps and triceps activity.

Acknowledgment

The authors would like to thank the anonymous reviewers for their useful comments, which improved the manuscript. R. Ronsse, N. Vitiello, and T. Lenzi contributed equally to this work.

References

[1] S. Schaal, "The new robotics—Towards human-centered machines," *HFSP J.*, vol. 1, no. 2, pp. 115–26, 2007.

[2] A. Dollar and H. Herr, "Lower extremity exoskeletons and active orthoses: Challenges and state-of-the-art," *IEEE Trans. Robot.*, vol. 24, no. 1, pp. 144–158, Feb. 2008.

[3] D. P. Ferris. (2009). The exoskeletons are here. *J Neuroeng. Rehabil.* [Online]. *6*, p. 17. Available: http://dx.doi.org/10.1186/1743-0003-6-17

[4] A. Zoss, H. Kazerooni, and A. Chu, "Biomechanical design of the berkeley lower extremity exoskeleton (bleex)," *IEEE/ASME Trans. Mechatronics*, vol. 11, no. 2, pp. 128–138, Apr. 2006.

[5] R. Riener, L. Lünenburger, S. Jezernik, M. Anderschitz, G. Colombo, and V. Dietz. (2005, Sep.). Patient-cooperative strategies for robot-aided treadmill training: first experimental results. *IEEE Trans. Neural Syst. Rehabil. Eng.* [Online]. *13(3)*, pp. 380–394. Available: http://dx.doi.org/10.1109/TNSRE.2005.848628

[6] H. Vallery, E. H. F. van Asseldonk, M. Buss, and H. van der Kooij. (2009, Feb.). Reference trajectory generation for rehabilitation robots: complementary limb motion estimation. *IEEE Trans. Neural Syst. Rehabil. Eng.* [Online]. *17(1)*, pp. 23–30. Available: http://dx.doi.org/10.1109/TNSRE.2008.2008278

[7] H. Kawamoto and Y. Sankai, "Power assist method based on phase sequence and muscle force condition for HAL," *Adv. Robot.*, vol. 19, no. 7, pp. 717–734, 2005.

[8] B. Dellon and Y. Matsuoka, "Prosthetics, exoskeletons, and rehabilitation [grand challenges of robotics]," *IEEE Robot. Autom. Mag.*, vol. 14, no. 1, pp. 30–34, Mar. 2007.

[9] W. B. Griffin, W. R. Provancher, and M. R. Cutkosky, "Feedback strategies for telemanipulation with shared control of object handling forces," *Presence*, vol. 14, no. 6, pp. 720–731, 2005.

[10] K. E. Gordon and D. P. Ferris. (2007). Learning to walk with a robotic ankle exoskeleton. *J. Biomech.* [Online]. *40(12)*, pp. 2636–2644. Available: http://dx.doi.org/10.1016/j.jbiomech.2006.12.006

[11] M. A. Nicolelis. (2001, Jan.). Actions from thoughts. *Nature.* [Online]. *409(6818)*, pp. 403–407. Available: http://dx.doi.org/10.1038/35053191

[12] M. Velliste, S. Perel, M. C. Spalding, A. S. Whitford, and A. B. Schwartz. (2008, Jun.). Cortical control of a prosthetic arm for self-feeding. *Nature.* [Online]. *453(7198)*, pp. 1098–1101. Available: http://dx.doi.org/10.1038/nature06996

[13] J. M. Carmena, M. A. Lebedev, R. E. Crist, J. E. O'Doherty, D. M. Santucci, D. F. Dimitrov, P. G. Patil, C. S. Henriquez, and M. A. L. Nicolelis. (2003, Nov.). Learning to control a brain-machine interface for reaching and grasping by primates. *PLoS Biol.* [Online]. *1(2)*. pp. E42. Available: http://dx.doi.org/10.1371/journal.pbio.0000042

[14] P. M. Rossini, S. Micera, A. Benvenuto, J. Carpaneto, G. Cavallo, L. Citi, C. Cipriani, L. Denaro, V. Denaro, G. D. Pino, F. Ferreri, E. Guglielmelli, K.-P. Hoffmann, S. Raspopovic, J. Rigosa, L. Rossini, M. Tombini, and P. Dario. (2010, May). Double nerve intraneural interface implant on a human amputee for robotic hand control. *Clin. Neurophysiol.* [Online]. *121(5)*. pp. 777–783. Available: http://dx.doi.org/10.1016/j.clinph.2010.01.001

[15] M. A. Lebedev and M. A. L. Nicolelis. (2006, Sep.). Brain-machine interfaces: past, present and future. *Trends Neurosci.* [Online]. *29(9)*, pp. 536–546. Available: http://dx.doi.org/10.1016/j.tins.2006.07.004

[16] J. Rosen, M. Brand, M. B. Fuchs, and M. Arcan, "A myosignal-based powered exoskeleton system," *IEEE Trans. Syst., Man Cybern. A*, vol. 31, no. 3, pp. 210–222, May 2001.

[17] K. Kiguchi, K. Iwami, M. Yasuda, K. Watanabe, and T. Fukuda, "An exoskeletal robot for human shoulder joint motion assist," *IEEE/ASME Trans. Mechatronics*, vol. 8, no. 1, pp. 125–135, Mar. 2003.

[18] E. Cavallaro, J. Rosen, J. Perry, and S. Burns, "Real-time myoprocessors for a neural controlled powered exoskeleton arm," *IEEE Trans. Biomed. Eng.*, vol. 53, no. 11, pp. 2387–2396, Nov. 2006.

[19] C. Kinnaird and D. Ferris, "Medial gastrocnemius myoelectric control of a robotic ankle exoskeleton," *IEEE Trans. Neural Syst. Rehabil. Eng.*, vol. 17, no. 1, pp. 31–37, Feb. 2009.

[20] G. S. Sawicki and D. P. Ferris. (2008, May). Mechanics and energetics of level walking with powered ankle exoskeletons. *J. Exp. Biol.* [Online]. *211(9)*, pp. 1402–1413. Available: http://dx.doi.org/10.1242/jeb.009241
[21] S. H. Strogatz, *Sync: The Emerging Science of Spontaneous Order*. New York: Hyperion, 2003.
[22] J. Duysens and H. W. Van de Crommert, "Neural control of locomotion; the central pattern generator from cats to humans," *Gait Posture*, vol. 7, no. 2, pp. 131–141, 1998.
[23] S. Schaal, D. Sternad, R. Osu, and M. Kawato, "Rhythmic arm movement is not discrete," *Nat. Neurosci.*, vol. 7, no. 10, pp. 1136–1143, 2004.
[24] E. P. Zehr and J. Duysens. (2004, Aug.). Regulation of arm and leg movement during human locomotion. *Neuroscientist* [Online]. *10(4)*, pp. 347–361. Available: http://dx.doi.org/10.1177/1073858404264680
[25] O. White, Y. Bleyenheuft, R. Ronsse, A. M. Smith, J.-L. Thonnard, and P. Lefèvre. (2008, Nov.). Altered gravity highlights central pattern generator mechanisms. *J. Neurophysiol.* [Online]. *100(5)*, pp. 2819–2824. Available: http://dx.doi.org/10.1152/jn.90436.2008
[26] R. Ronsse, D. Sternad, and P. Lefèvre. (2009, May). A computational model for rhythmic and discrete movements in uni- and bimanual coordination. *Neural Comput.* [Online]. *21(5)*, pp. 1335–1370. Available: http://dx.doi.org/10.1162/neco.2008.03-08-720
[27] L. Righetti, J. Buchli, and A. J. Ijspeert, "Dynamic hebbian learning in adaptive frequency oscillators," *Physica D*, vol. 216, pp. 269–281, 2006.
[28] L. Righetti, J. Buchli, and A. J. Ijspeert, "Adaptive frequency oscillators and applications," *Open Cybern. Systemics J.*, vol. 3, pp. 64–69, 2009.
[29] J. Buchli, F. Iida, and A. J. Ijspeert, "Finding resonance: Adaptive frequency oscillators for dynamic legged locomotion," in *Proc. IEEE/RSJ Int. Conf. Intell. Robots Syst.*, Oct. 9–15., 2006, pp. 3903–3909.
[30] J. Buchli, L. Righetti, and A. J. Ijspeert, "Frequency analysis with coupled nonlinear oscillators," *Physica D*, vol. 237, pp. 1705–1718, 2008.
[31] L. Righetti and A. J. Ijspeert, "Programmable central pattern generators: An application to biped locomotion control," in *Proc. IEEE Int. Conf. Robot. Autom. ICRA 2006*, May 15–19, pp. 1585–1590.
[32] A. Gams, A. J. Ijspeert, S. Schaal, and J. Lenarčič, "On-line learning and modulation of periodic movements with nonlinear dynamical systems," *Auton. Robot.*, vol. 27, pp. 3–23, 2009.
[33] A. Goswami, B. Thuilot, and B. Espiau, "A study of the passive gait of a compass-like biped robot: Symmetry and chaos," *Int. J. Robot. Res.*, vol. 17, no. 12, pp. 1282–1301, 1998.
[34] R. Ronsse, N. Vitiello, T. Lenzi, J. van den Kieboom, M. C. Carrozza, and A. J. Ijspeert, "Adaptive oscillators with human-in-the-loop: Proof of concept for assistance and rehabilitation," in *Proc. 3rd IEEE RAS EMBS Int. Conf. Biomed. Robot. Biomechatron.—BIOROB 2010*, pp. 668–674.
[35] D. A. Winter, *Biomechanics and Motor Control of Human Movement*, 4th ed. ed. Hoboken, NJ: Wiley, 2009.
[36] C.-C. Lin, M.-S. Ju, and C.-W. Lin. (2003, Jan.). The pendulum test for evaluating spasticity of the elbow joint. *Arch. Phys. Med. Rehabil.* [Online]. *84(1)*, pp. 69–74. Available: http://dx.doi.org/10.1053/apmr.2003.50066
[37] T. Lenzi, S. De Rossi, N. Vitiello, A. Chiri, S. Roccella, F. Giovacchini, F. Vecchi, and M. C. Carrozza, "The neuro-robotics paradigm: NEURARM, NEUROExos, HANDEXOS," in *Proc. Annu. Int. Conf. IEEE Eng. Med. Biol. Soc., EMBC 2009*, Sep. 3–6, pp. 2430–2433.
[38] N. Vitiello, "The NEURO-ROBOTICS paradigm three case-study platform: The robotic arm NEURARM, the elbow exoskeleton NEUROExos, and a tactile stimulator for touch studies," Ph.D. dissertation, Scuola Superiore Sant'Anna, Italy, 2010.
[39] T. R. Duck, C. E. Dunning, G. J. W. King, and J. A. Johnson. (2003, May). Variability and repeatability of the flexion axis at the ulnohumeral joint. *J. Orthop. Res.* [Online]. *21(3)*, pp. 399–404. Available: http://dx.doi.org/10.1016/S0736-0266(02)00198-5
[40] G. A. Pratt and M. M. Williamson, "Series elastic actuators," in *Proc. IEEE/RSJ Int. Conf. Intell. Robots Syst., Human Robot Interaction Cooperative Robots*, Aug. 5–9, 1995, vol. 1, pp. 399–406.
[41] M. Zinn, B. Roth, O. Khatib, and J. K. Salisbury. (2004). A new actuation approach for human friendly robot design. *Int. J. Robot. Res.* [Online]. *23(4–5)*, pp. 379–398. Available: http://ijr.sagepub.com/cgi/content/abstract/23/4-5/379
[42] H. Vallery, J. Veneman, E. van Asseldonk, R. Ekkelenkamp, M. Buss, and H. van Der Kooij, "Compliant actuation of rehabilitation robots," *IEEE Robot. Autom. Mag.*, vol. 15, no. 3, pp. 60–69, Sep. 2008.
[43] N. Vitiello, T. Lenzi, J. McIntyre, S. Roccella, E. Cattin, F. Vecchi, and M. C. Carrozza. (2008, Oct.). 'Characterization of the NEURARM bio-inspired joint position and stiffness open loop controller," in *Proc. 2008 2nd IEEE RAS EMBS Int. Conf. Biomed. Robot. Biomechatron.*, pp. 138–143, [Online]. Available: http://ieeexplore.ieee.org/lpdocs/epic03/wrapper.htm?arnumber=4762817
[44] N. Vitiello, T. Lenzi, S. M. M. De Rossi, S. Roccella, and M. C. Carrozza. (2010, Apr.). A sensorless torque control for antagonistic driven compliant joints, *Mechatronics.* [Online]. *20(3)*, pp. 355–367. Available: http://dx.doi.org/10.1016/j.mechatronics.2010.02.001
[45] D. Aoyagi, W. Ichinose, S. Harkema, D. Reinkensmeyer, and J. Bobrow, "A robot and control algorithm that can synchronously assist in naturalistic motion during body-weight-supported gait training following neurologic injury," *IEEE Trans. Neural Syst. Rehabil. Eng.*, vol. 15, no. 3, pp. 387–400, Sep. 2007.
[46] A. D. Kuo, "The relative roles of feedforward and feedback in the control of rhythmic movements," *Motor Control*, vol. 6, no. 2, pp. 129–145, 2002.
[47] C. J. Walsh, K. Endo, and H. Herr, "A quasi-passive leg exoskeleton for load-carrying augmentation," *Int. J. Humanoid Robot.*, vol. 4, no. 3, pp. 487–506, 2007.
[48] G. S. Sawicki and D. P. Ferris. (2009, Jan.). Powered ankle exoskeletons reveal the metabolic cost of plantar flexor mechanical work during walking with longer steps at constant step frequency. *J. Exp. Biol.* [Online]. *212(Pt 1)*, pp. 21–31. Available: http://dx.doi.org/10.1242/jeb.017269
[49] R. Shadmehr and F. A. Mussa-Ivaldi, "Adaptive representation of dynamics during learning of a motor task.," *J. Neurosci.*, vol. 14, no. 5(Pt 2), pp. 3208–3224, May 1994.
[50] R. Shadmehr and S. P. Wise, *The Computational Neurobiology of Reaching and Pointing. A Foundation for Motor Learning*. Cambridge, MA: MIT Press, 2005.
[51] J. Izawa, T. Rane, O. Donchin, and R. Shadmehr. (2008, Mar.). Motor adaptation as a process of reoptimization. *J. Neurosci.* [Online]. *28(11)*, pp. 2883–2891. Available: http://dx.doi.org/10.1523/JNEUROSCI.5359-07.2008
[52] E. H. F. Van Asseldonk, R. Ekkelenkamp, J. F. Veneman, F. C. T. Van der Helm, and H. van der Kooij, "Selective control of a subtask of walking in a robotic gait trainer(lopes)," in *Proc. IEEE 10th Int. Conf. Rehabil. Robot., ICORR 2007*, Jun., 13–15, pp. 841–848.
[53] A. Duschau-Wicke, J. von Zitzewitz, A. Caprez, L. Lunenburger, and R. Riener, "Path control: A method for patient-cooperative robot-aided gait rehabilitation," *IEEE Trans. Neural Syst. Rehabil. Eng.*, vol. 18, no. 1, pp. 38–48, Feb. 2010.
[54] S. Jezernik, G. Colombo, and M. Morari, "Automatic gait-pattern adaptation algorithms for rehabilitation with a 4-dof robotic orthosis," *IEEE Trans. Robot. Autom.*, vol. 20, no. 3, pp. 574–582, Jun. 2004.
[55] E. T. Wolbrecht, V. Chan, D. J. Reinkensmeyer, and J. E. Bobrow. (2008, Jun.). Optimizing compliant, model-based robotic assistance to promote neurorehabilitation. *IEEE Trans. Neural Syst. Rehabil. Eng.* [Online]. *16(3)*, pp. 286–297. Available: http://dx.doi.org/10.1109/TNSRE.2008.918389
[56] C. B. Hart and S. F. Giszter. (2010, Jan.). A neural basis for motor primitives in the spinal cord. *J. Neurosci.* [Online]. *30(4)*, pp. 1322–1336. Available: http://dx.doi.org/10.1523/JNEUROSCI.5894-08.2010
[57] S. Dégallier and A. Ijspeert. (2010, Oct.). Modeling discrete and rhythmic movements through motor primitives: A review. *Biol. Cybern.* [Online]. *103(4)*, pp. 319–338. Available: http://dx.doi.org/10.1007/s00422-010-0403-9
[58] A. Ijspeert, J. Nakanishi, and S. Schaal, "Learning attractor landscapes for learning motor primitives," in *Advances in Neural Information Processing Systems*, vol. 15, Cambridge, MA: MIT Press, 2003, pp. 1547–1554.
[59] R. Ronsse, K. Wei, and D. Sternad. (2010, May). Optimal control of a hybrid rhythmic-discrete task: The bouncing ball revisited. *J. Neurophysiol.* [Online]. *103(5)*, pp. 2482–2493. Available: http://dx.doi.org/10.1152/jn.00600.2009

Renaud Ronsse received the M.Sc. and Ph.D. degrees in electrical engineering from the Université de Liège, Liege, Belgium, in 2002 and 2007, respectively. His thesis was focused on the control of rhythmic movements involving hybrid dynamics (impact juggling), investigating both robotics and human motor control issues.

He was a Postdoctoral Fellow at the Katholieke Universiteit Leuven, engaged in the research on behavioral and neural mechanisms involved in bimanual coordination. He is currently a Postdoctoral Fellow at Biorobotics Laboratory, École Polytechnique Fédérale de Lausanne (EPFL), Switzerland. In 2011, He will join the Center for Research in Mechatronics, Université catholique de Louvain, as an Assistant Professor. His research interests include the intersection between robotics and human motor control, with a particular focus on assistive and rehabilitation robotics.

Nicola Vitiello received the M.Sc. degree in biomedical engineering (*cum laude*) from the University of Pisa, Pisa, Italy, in July 2006. He is currently working toward the Ph.D. degree in biorobotics at Scuola Superiore Sant'Anna, Pisa.

He is involved in research at the Advanced Robotics Technology and System (ARTS) Laboratory, Scuola Superiore Sant'Anna. His current research interests include the development of control algorithms for biorobotics platforms for investigating neuroscience issues. In 2006, he participated at the IX European Space Agency (ESA) Student Parabolic Flight Campaign as a team member. In 2008, he participated at the first ESA Lunar Robotics Challenge, as a Ph.D. Student Member of the team of Scuola Superiore Sant'Anna.

Tommaso Lenzi (S'10) received the M.Sc. degree in biomedical engineering (*cum laude*) from the University of Pisa, Pisa, Italy, in April 2008. He is currently working toward the Ph.D. degree at the Advanced Robotics Technology and System (ARTS) Laboratory, Scuola Superiore Sant'Anna, Pisa.

His current research interests include neurorobotics and bioengineering for upper and lower limb rehabilitation.

Jesse van den Kieboom received the M.Sc. degree in artificial intelligence (*cum laude*) from the University of Groningen, Groningen, The Netherlands, in April 2009. He is currently working toward the Ph.D. degree at the Biorobotics Laboratory, École Polytechnique Fédérale de Lausanne (EPFL), Switzerland.

At EPFL, he is involved in the research on the codesign of mechanics and control using co-evolutionary algorithms, more specifically for lower limb exoskeletons targeting assistance and rehabilitation.

Maria Chiara Carrozza (M'04–A'06) is a Full Professor of biomedical engineering and robotics at Scuola Superiore Sant'Anna (SSSA), Pisa, Italy. Since November 2007, she has been the Director of Scuola Superiore Sant'Anna. She was a Visiting Professor at the Technical University of Wien, Austria, with a graduate course entitled Biomechatronics, and she is involved in the scientific management of the Italy–Japan joint laboratory for Humanoid Robotics ROBOCASA, Waseda University, Tokyo. She is the author of several scientific papers (more than 60 ISI papers and more than 100 papers in referred conference proceedings) and holds 12 national and international patents. Her research interests include ambient assisted living, technical aids, biorobotics, rehabilitation engineering, bionics, cybernetic hands, humanoid robotics, systems for functional replacements and augmentation, biomechatronic interfaces, tactile sensors, artificial skin, applications of renewable energy to robotics, and robotics to renewable energy.

Auke Jan Ijspeert (M'00) received the B.Sc. and M.Sc. degrees in physics from École Polytechnique Fédérale de Lausanne (EPFL), Switzerland, and the Ph.D. degree in artificial intelligence from the University of Edinburgh, Edinburgh, U.K..

He is a Professor at EPFL (the Swiss Federal Institute of Technology in Lausanne), and the Head of the Biorobotics Laboratory. His research interests include the intersection among robotics, computational neuroscience, nonlinear dynamical systems, and applied machine learning; using numerical simulations and robots to get a better understanding of sensorimotor coordination in animals; and in using inspiration from biology to design novel types of robots and adaptive controllers.

Dr. Ijspeert (with his colleagues) received the Best Paper Award at the IEEE International Conference on Robotics and Automation (ICRA2002), the Industrial Robot Highly Commended Award at International Conference on Climbing and Walking Robots (CLAWAR) 2005, and the Best Paper Award at the IEEE Robotics and Automation Society (IEEE-RAS) Humanoids 2007 conference. He was the Technical Program Chair of five international conferences (International Workshop on Biologically Inspired Approaches to Advanced Information Technology (BioADIT) 2004, International Conference on the Simulation of Adaptive Behavior 2004, International Symposium on Adaptive Motion in Animals and Machines 2005, BioADIT2006, LATSIS2006), and has been a Program Committee Member of more than 40 conferences.